



Numerical Acoustic Modelling of Cross-Laminated Timber Elements

Sven Vallely¹, Stefan Schoenwald¹

¹Laboratory for Acoustics / Noise Control, Swiss Federal Laboratories for Materials Science and Technology (Empa),
Dübendorf, Switzerland.

sven.vallely@empa.ch, stefan.schoenwald@empa.ch

Abstract

Cross-Laminated Timber (CLT) has shown great promise in recent years as a renewable, sustainable, and cost-efficient building material. However, due to CLT's relatively low mass and high stiffness, CLT's airborne and impact sound insulation performance has proven to be less than optimal. Fundamental to addressing this shortcoming and ensuring the success of CLT, the development of computationally efficient acoustic models that are functions of the geometry, orientation, and stacking sequence of the plies with predetermined material properties are critical. Such models will ensure the possibility for rapid and cost-effective exploration of the effective design space in order to overcome CLT's acoustic shortcoming. To date, not a large amount of literature exists on acoustic related Finite Element Analysis (FEA) of CLT. Of the literature that exists, the focus has been on the low frequency range, due to the high computational demand of modelling thick laminated structures. This paper presents a validated FEA approach to CLT, which allows for computationally efficient and accurate broadband acoustic modelling in the context of building acoustic problems.

Keywords: Cross-Laminated Timber (CLT), Finite Element Method (FEM), Vibro-acoustics, Structural Dynamics, Numerical Modelling

1 Introduction

The growth of CLT in the building industry has been significantly increasing in recent years [1]. A driver of CLTs growth in addition to its environmental, economic, and sustainability benefits is CLT's mechanical properties. CLT has a relatively high stiffness for its mass density, which is highly beneficial for static structural applications. However, such mechanical properties that are ideal for static structural applications directly result in a poorer overall sound insulation performance [2]. To overcome these acoustic limitations, the development of computationally efficient acoustic models that are functions of geometry, orientation, and stacking sequences of the plies with predetermined material properties is critical. Such models can be utilised to explore the effective design space in order to overcome CLT's acoustic shortcoming.

The Finite Element Method (FEM), which is a very flexible analysis method with the ability to model arbitrarily complex boundary conditions and geometries has already been applied to CLT. However, the method can be very computationally demanding, and therefore, there is a lack of experimentally validated computationally efficient models that extend beyond the low-frequency range [3]. More efficient hybrid solutions that were explored so far are a FEM / Statistical Energy Analysis method [4], and the Wave Finite Element Method [5], which have been numerically or experimentally investigated. Both approaches have their drawbacks, such as inaccuracies due to the requirement for homogenisation of the layers, infinite plate assumptions, and a lack of experimental validation or discrepancies between the numerical and experimental results.

Efficient modelling techniques in FEM can extend FEM models from the low- to the mid- and high-frequency ranges while retaining the flexibility and accuracy of FEM modelling. This contribution puts forwards ideas to achieve computationally efficient broadband models for CLT in the context of building acoustics with FEM. Layerwise experimentally validated shell and solid element models are presented. These models are benchmarked with considerations such as solution method, and solution intervals for time-harmonic analyses. Further, consideration is given to the influence of older and newer hardware on the runtime of these models.

2 Analysis and Evaluation Tools

2.1 Spatially Averaged Squared Velocity

For broadband analyses in vibro-acoustics, it can be cumbersome to deal with the responses of the individual eigenfrequencies and associated eigenmodes, since potentially thousands of these eigenfrequency-eigenmode pairs are required to constitute the broadband response of the system. Therefore, the spatial average of the square of the surface response velocity $\overline{|v|^2}$ is a useful metric for broadband analyses. $\overline{|v|^2}$ is defined as [6],

$$\overline{|v|^2} = \frac{1}{m_{tot}} \iint \rho_A(x, y) |v(x, y)|^2 dx dy. \quad (1)$$

$|v|^2$ is equal to the total energy of the vibrating system divided by the total mass m_{tot} of the vibrating system. The function $\rho_A(x, y)$ is the area mass density and $v(x, y)$ is the complex velocity distribution of the system. For a point force excitation, $\overline{|v|^2}$ is directly dependent on the summation of the eigenfunctions and angular eigenfrequencies, the proximity of the angular excitation frequency to the individual eigenfrequencies, and the location of the point force [6]. $|v|^2$ is also directly proportional to the radiated sound power of the system at a given frequency [6].

In the following studies, $|v|^2$ is normalised by the square of the modulus of the point excitation force,

$$\overline{|Y(\omega)|^2} = \frac{\overline{|v(\omega)|^2}}{\overline{|F_1(\omega)|^2}}. \quad (2)$$

$\overline{|Y(\omega)|^2}$ is the spatially averaged squared transfer mobility.

3 Method

3.1 Experiment

The CLT plate considered in this work was a 5-ply plate with dimensions 5.73 m \times 2.38 m \times 0.200 m including an approximately 100 mm half lap joint. The stacking sequence of the plate was $[0/90/\bar{0}]_5$ with 40.0 mm thick plies. In order to emulate free boundary conditions, the plate was supported by three air jacks as depicted in Figure 1. It was dynamically excited on the underside with an inertial shaker using a sine sweep signal. The inertial shaker is circled in red in Figure 1a. The plate was excited at three different points to ensure that all of the modes of interest were adequately excited. The three excitation points are depicted schematically in Figure 1b as F_1 , F_2 , and F_3 . Excitation point F_1 is considered for the benchmarking studies in this paper. In Figure 1b, where the lower left-hand corner of the plate has the planar coordinates (0 m, 0 m), the planar coordinates of the excitation point F_1 was (0.04 m, 0.05 m). The surface velocity of the topside of the plate was measured from above with a Polytech Scanning Laser Doppler Vibrometer on a rectangular 16 \times 39 grid of points, as depicted approximately in Figure 1b.

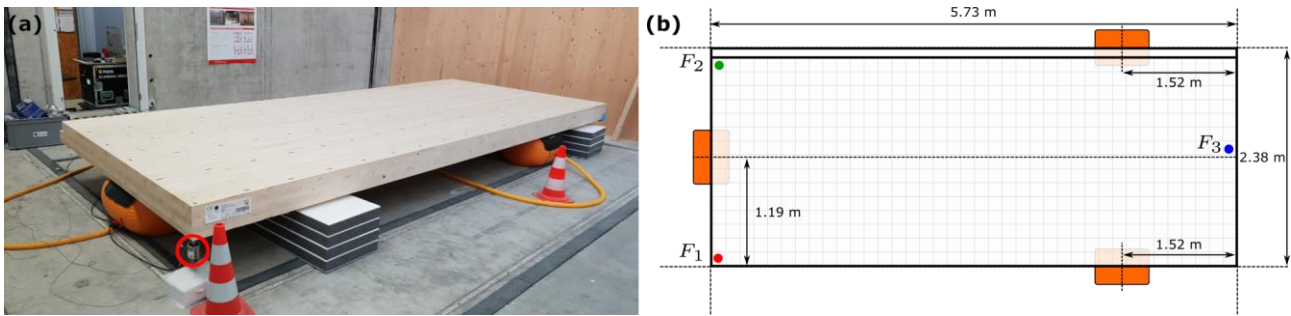


Figure 1 – Experimental set-up. (a) Photo of the experimental set-up. (b) 2D schematic indicating the plate dimensions, air-jack support locations, approximate measurement grid, and location of the three excitation points F_1 , F_2 , and F_3 .

3.2 Numerical Modelling

The CLT plate is modelled numerically using FEM with Ansys Academic Research Mechanical, Release 2020 R2. In the numerical modelling of the geometry and the material properties of the CLT plate, each layer is assumed to be homogenous and orthotropic. The geometry of the CLT plate was represented and analysed in two different ways as presented in Figure 2. The first method, in Figure 2a, involved a two-dimensional (2D) representation where the layers are implicitly modelled. This 2D representation was discretised with a mapped quadrilateral mesh, as shown in Figure 2c. The second method, in Figure 2b, involved a three-dimensional (3D) representation with explicitly modelled layers. This 3D representation was discretised with a mapped hexahedral mesh, as shown in Figure 2d. The global mesh size was 40 mm for both the 2D and 3D geometries. This global mesh size corresponded to one element through the thickness of each layer in the 3D geometry.

For modelling the orthotropic elastic material properties of CLT. The Ansys shell element SHELL281 and solid element SOLID186 were chosen for the 2D and 3D geometries respectively. Both elements have the option for orthotropic material definitions and are depicted in Figure 3a and Figure 3b respectively. The orientation of the layers of the CLT plate – $[0/90/\bar{0}]_S$ – for the SHELL281 and SOLID186 models are depicted schematically in Figure 3c. The orthotropic elastic material properties of the layers were obtained via a model updating process using SHELL281 elements. The objective function was defined as the root mean square difference of numerical and experimental eigenfrequencies weighted by their respective modal assurance criterion value, which was then minimised with a gradient-based single-objective optimisation algorithm. The density of the plate was derived from weighing the plate and the material damping was derived using the Power Injection Method [6]. The applied material properties are presented in Table 1.

Time-harmonic structural dynamic analyses were conducted for both of the models with free boundary conditions. Both the Mode-Superposition (MSUP) and the Full harmonic (FULL) analysis methods were considered. The parameters used for the validation and benchmark studies are summarised in Table 2 and Table 3 respectively. Linear and logarithmic solution intervals were considered for the benchmark studies. The harmonic excitation force of the inertial shaker was modelled as a point force on the node nearest to the physical location. The point force was set as 1 N in order to directly obtain the transfer mobility function. The models were benchmarked across two workstations with the general hardware specification of the workstations summarised in Table 4. All of the solutions were set to run in-core with distributed memory parallel on 4-cores.

For post-processing, the velocity of each node on the measurement surface of the plate was extracted as a function of frequency. The surface velocity response of the nodes were then mapped using two-dimensional linear interpolation to the points on the experimental measurement grid. Lastly, the spatially average squared transfer mobilities were calculated for direct comparison with the experimental results.

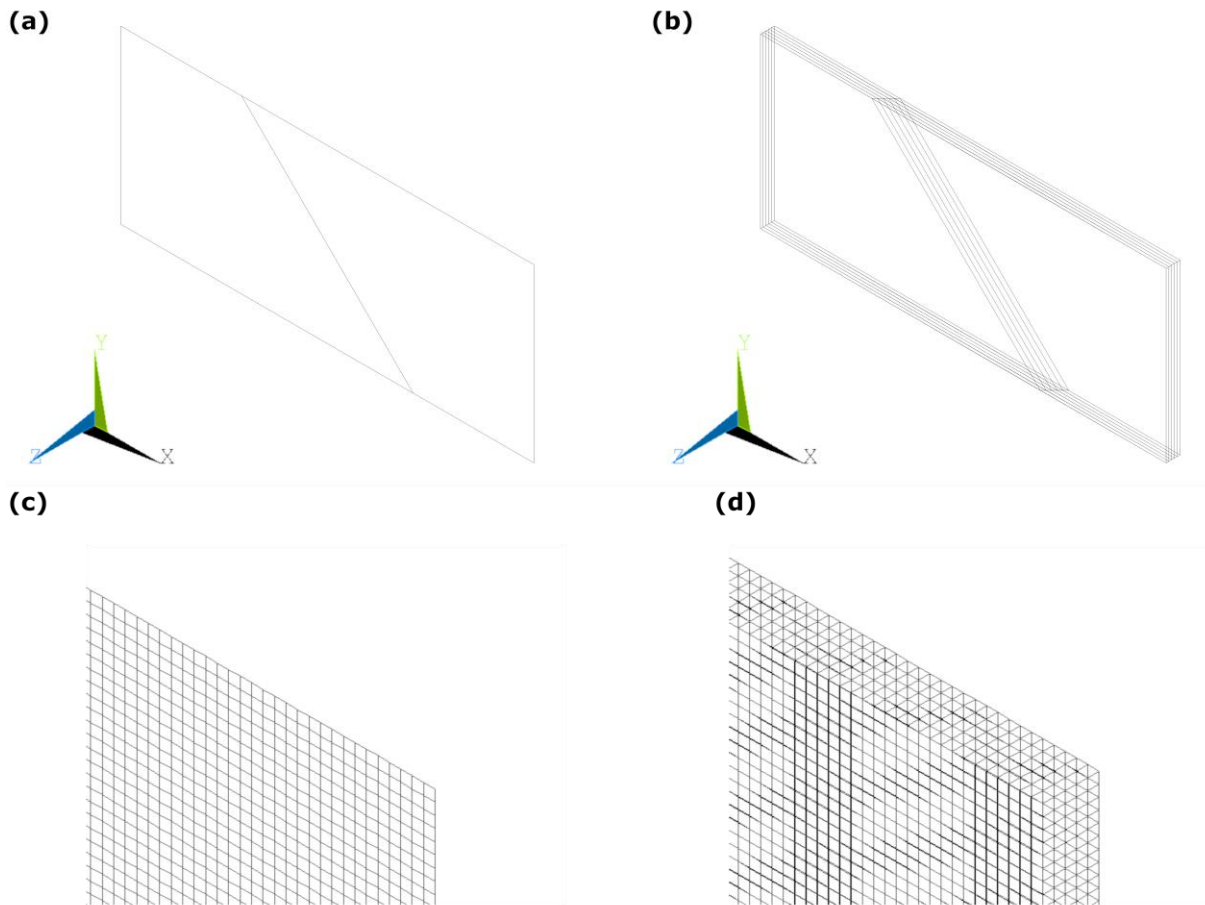


Figure 2 – Wireframe representation of the CLT plate with continuous and discretised (meshed) geometries. (a) 2D continuous representation with cross-section diagonally inset. (b) 3D continuous representation with cross-section diagonally inset. (c) 2D discretised geometry with a mapped quadrilateral mesh. (d) 3D discretised geometry with a mapped hexahedral mesh.

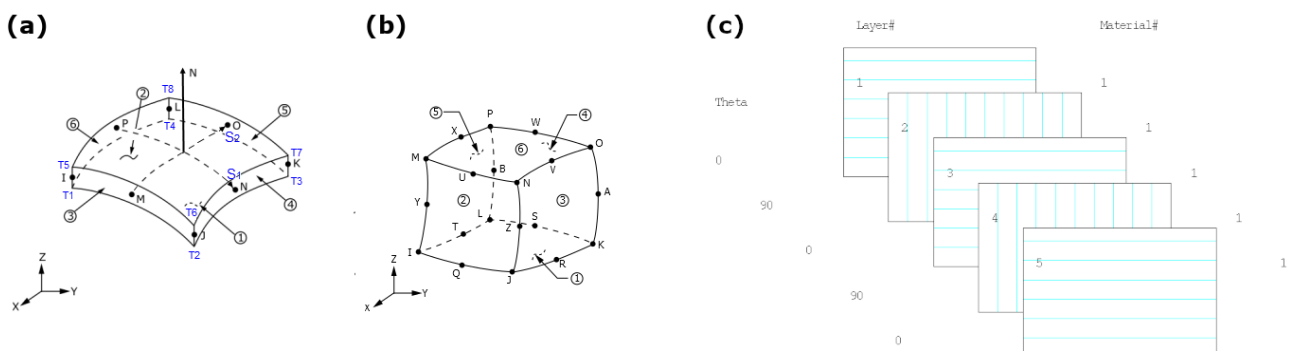


Figure 3 – Utilised elements and the orientations of the layers of the CLT plate. (a) SHELL281: 8-node structural shell element [7]. (b) SOLID186: 20-node structural solid element [7]. (c) Schematic depicting the implemented layer-orientations of the CLT plate.

Table 1 – Material properties of the CLT plate layers.

Density ρ (kg.m ⁻³)	Damping Ratio ζ (1)	Elastic Moduli (GPa)			Poisson's Ratio (1)			Shear Moduli (GPa)		
		E_x	E_y	E_z	ν_{xy}	ν_{yz}	ν_{xz}	G_{xy}	G_{yz}	G_{xz}
444	0.00850	11.8	0.999	0.999	0.100	0.300	0.100	0.748	0.176	0.538

Table 2 – Parameter settings for the harmonic analysis validation studies.

Element	Analysis	No. of Modes Extracted (1)	Frequency Range		
			Beginning (Hz)	End (Hz)	No. Substeps (1)
SHELL281	MSUP	1800	0	177.5	2840
	FULL	N/A	177.5	3565	2710
SOLID186	MSUP	1800	0	177.5	2840
	FULL	N/A	177.5	3565	2710

Table 3 – Parameter settings for the harmonic analysis benchmark studies.

Element	Analysis	No. of Modes Extracted (1)	Frequency Range (Linear / Log)		
			Beginning (Hz)	End (Hz)	No. Substeps (1)
SHELL281	MSUP	1800			
	FULL	N/A			
SOLID186	MSUP	1800	0 / 10	3565 / 3565	2852 / 700
	FULL	N/A			

Table 4 – General specifications of the workstations used for benchmarking the models.

Computer ID	A	B
Central Processing Unit (CPU)	Manufacturer	Intel
	Model	2 × Xeon CPU E5-2620 v2
	No. Cores (1)	12 (2 × 6)
	Launch Date	2.10 Q3 2013
Random Access Memory (RAM)	Manufacturer	Kingston / Hynix
	Type	DDR3
	Capacity (GB)	96 (12 × 8 GB)
	Config. Clock Speed (MHz)	1600
Storage	Manufacturer	Samsung
	Model(s)	970 EVO Plus NVMe SSD
	Capacity (TB)	2
Operating System	Edition	Windows 10 Education
	Version	1909

4 Results and Discussion

4.1 Model Validation

The spatially averaged squared transfer mobilities derived from experiment and simulation excited at F_1 (Sec. 3.1) are plotted in Figure 4. A frequency range from 17 Hz to 3564 Hz is considered. This frequency range captures the response of the first mode at approximately 19 Hz and the overall low-, mid-, and high-frequency dynamic response of the plate.

Considering the left-hand axis of Figure 4a, the $\overline{|Y|^2}$ levels of the experiment and simulation with SHELL281 elements are plotted. The $\overline{|Y|^2}$ values are seen to have an excellent agreement until approximately 500 Hz. From 500 Hz until 2000 Hz, there is a very good agreement with the overall $\overline{|Y|^2}$ levels, however, the peaks and troughs do not always line up. From 2000 Hz onwards, there is a divergence in the $\overline{|Y|^2}$ levels. However, this divergence between the experimental and simulation results can be attributed to an inaccurate force reading during the experiment. Considering the right-hand axis in Figure 4a, input force levels at the excitation point are plotted. This input force was used to derive the experimental $\overline{|Y|^2}$ levels. The signal appears to be relatively smooth and have little noise from 17 Hz to 2000 Hz. From 2000 Hz onwards, the signal appears to be noisy, and an inverse relationship is evident between the input force and the $\overline{|Y|^2}$ levels. This inaccuracy of the reading is likely due to the contact interface of the transducer mounting.

Considering Figure 4b, the $\overline{|Y|^2}$ levels from experiment and simulation with SOLID186 elements are plotted. Similar to the SHELL281 model presented in Figure 4a, an excellent agreement in the $\overline{|Y|^2}$ levels is seen from 17 Hz to 500 Hz. From 500 Hz until approximately 1800 Hz, there is a very good agreement with the overall $\overline{|Y|^2}$ levels, however the peaks and troughs do not always agree. From 1800 Hz until approximately 2800 Hz, the levels diverge and converge again. This divergence in $\overline{|Y|^2}$ levels can be attributed due to an inaccurate force reading during experiment, as discussed prior for Figure 4a. From 2800–3564 Hz, there is a very good agreement between the experiment and simulation levels. Comparing the simulation results of the SHELL281 and SOLID186 models in Figure 4a and Figure 4b respectively, $\overline{|Y|^2}$ responses of the models are seen to be very similar across most of the considered frequency range, but not identical. Considering the responses from 17–500 Hz, the SOLID186 elements appear to be stiffer than the SHELL281 elements. This difference in stiffness is likely due to the SOLID186 elements having only translational degrees of freedom while the SHELL281 elements have both translational and rotational degrees of freedom. From 500–1000 Hz, the SOLID186 model appears to be slightly more accurate, with the peaks and troughs lining up with those of the experimental slightly better than the SHELL281 model. From 1000–2000 Hz, the response of the SHELL281 model appears to be more accurate, with the $\overline{|Y|^2}$ levels more closely following those of the experiment than the SOLID186 model. From approximately 2800 Hz onwards, the SOLID186 elements are more accurate than the SHELL281 elements with the SHELL281 model underestimating the levels by approximately 10 dB. From 2800 Hz, the limitation of the 2.5-dimensional nature of the shell elements may be seen. The thickness modes have cut-on and their influence is now non-negligible. These thickness modes are not captured with the 2D geometry of the SHELL281 model, but are captured with the 3D geometry of the SOLID186 model. Overall, the SHELL281 is still very accurate for calculations including up until the nominal 2500 Hz octave band.

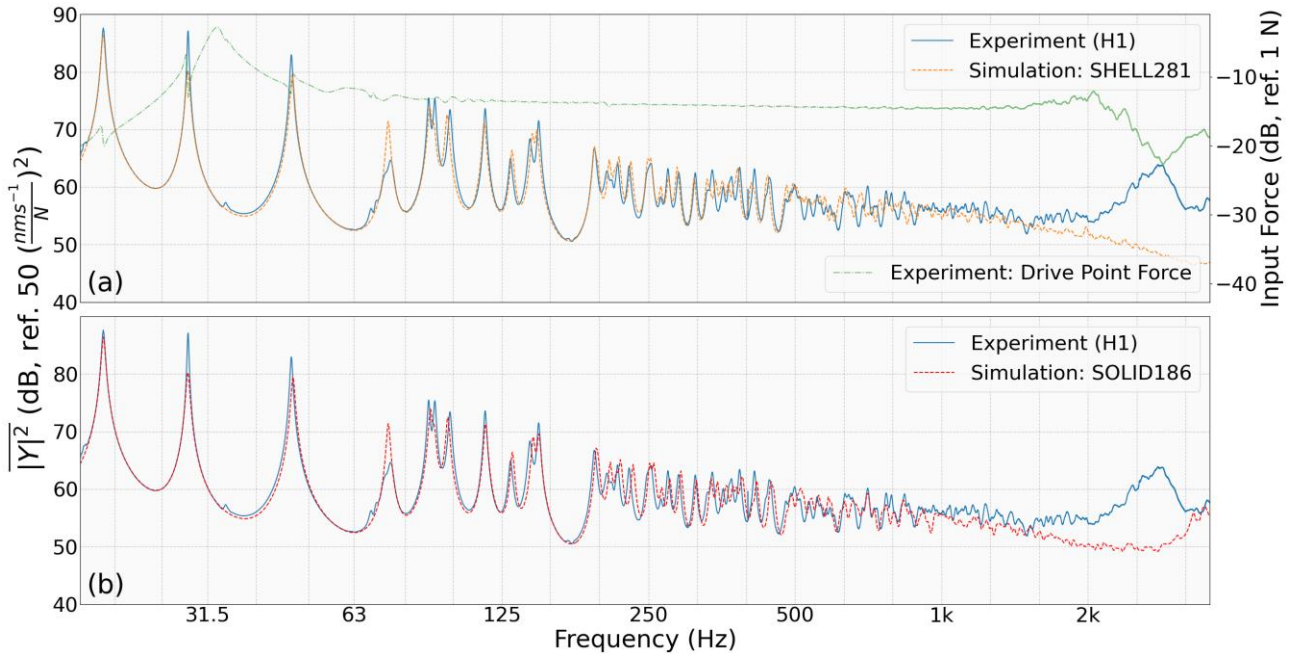


Figure 4 – Frequency response functions of experimental results and the validated FE models from 17 Hz to 3654 Hz for F_1 . Left axis: Experimental and numerical spatially averaged squared transfer mobilities ($|Y|^2$). Right axis: Measured experimental input force of the shaker at the excitation point. (a) SHELL281. (b) SOLID186.

4.2 Benchmarking

The $|Y|^2$ levels of the MSUP and FULL solution methods are presented in Figure 5 for the SHELL281 and SOLID186 models. The solution methods for both the SHELL281 model in Figure 5a and SOLID186 in Figure 5b have an excellent agreement until approximately 2500 Hz. From 2500 Hz, the values begin to slightly diverge, however, more so for the SHELL281 model. The divergence indicates a breakdown in the MSUP method for higher frequencies. The results may be improved slightly by using more modes with the MSUP, however, the authors found the increase in accuracy with respect to computational effort diminishing after 1800 Modes.

Table 5 presents a summary of the benchmarked simulations for the SHELL281 and SOLID186 models with MSUP and FULL solution methods on Computer A (Table 4). The SHELL281 model with the MSUP solution method was by far the fastest model requiring 33 minutes to run. This model also required the least amount of RAM to run in-core with a total of 683 MB required. The model that took the most amount of time to run was the SOLID186 model with the FULL solution method, requiring 99 hours 30 minutes to run. This model also required the most RAM of the models to run in-core, with a total of 13.8 GB required.

Table 6 presents the relative runtime and memory requirements of the models. The reference is the SHELL281 MSUP model. This model is a 181 factor improvement in runtime over a SOLID186 FULL model. The SOLID186 FULL model also requires a factor of 20 more memory for solving in-core. The second fastest model, the SOLID186 MSUP model had a runtime 5 times that of the SHELL281 MSUP model and 13 times the memory requirements. The third fastest model, SHELL281 FULL, was 13 times slower than SHELL281 MSUP and required twice the memory. While using shell elements in combination with a full solution method has a significant effect on the overall simulation time, the solution method has a greater effect than the element type.

Figure 6 presents the $\overline{|Y|^2}$ levels of the MSUP SHELL281 and SOLID186 models with linear and logarithmic solution intervals. The linear solution intervals are the same as those described in Table 2, and the logarithmic intervals are described Table 3. There is an excellent overall agreement, despite the logarithmic solution intervals having a far lower resolution in comparison to those of the linear solution intervals. Table 7 presents the solution times of the respective models with logarithmic solution intervals on Computer A and Computer B. A factor speed-up of approximately 2.5 is seen for the models, with the SHELL281 and SOLID186 models now requiring 12 and 67 minutes respectively to solve. In addition, comparing the respective models in Figure 5 and Figure 6, an improvement in the capturing of the $\overline{|Y|^2}$ levels is seen at low-frequencies for the logarithmic solution interval. On Computer B, another factor of 2 improvement in the runtimes is seen when solving the models. This improvement is likely due to the CPU on Computer B being 6.5 years newer than the CPU on Computer A. It is unlikely that the RAM or storage are the current bottlenecks on Computer A.

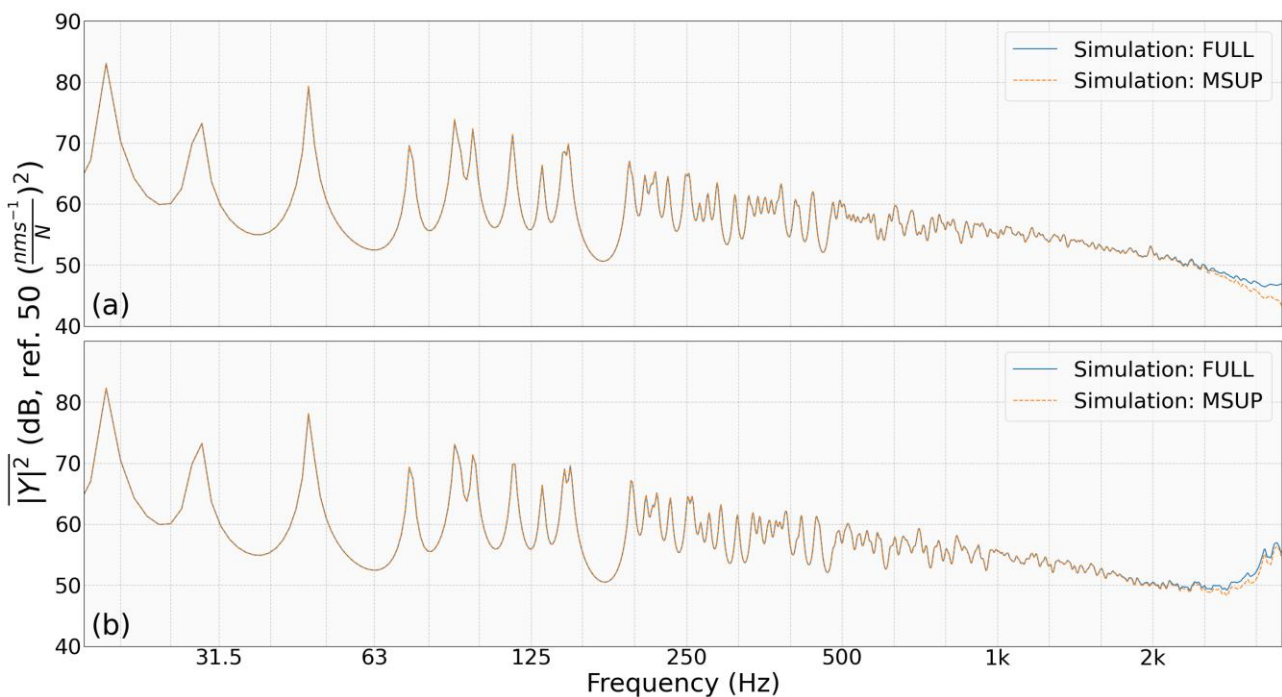


Figure 5 – Comparison of the mode-superposition (MSUP) and full solution (FULL) methods' spatially averaged squared transfer mobilities ($\overline{|Y|^2}$) from 17 Hz to 3654 Hz for F_1 . (a) SHELL281. (b) SOLID186.

Table 5 – Summary of the solution runtimes (Computer A) and minimum in-core memory requirements.

Element Type	Runtime (hr:min)	RAM Required (GB)
<i>Modal Superposition</i>		
SHELL281	0:33	0.683
SOLID186	2:30	8.20
<i>Full Method</i>		
SHELL281	7:10	1.22
SOLID186	99:30	13.8

Table 6 – Relative model runtime (Computer A) and minimum in-core memory requirements to the nearest whole number.

Method \ Element	SHELL281	SOLID186
MSUP	1 (1)	5 (13)
FULL	13 (2)	181 (20)

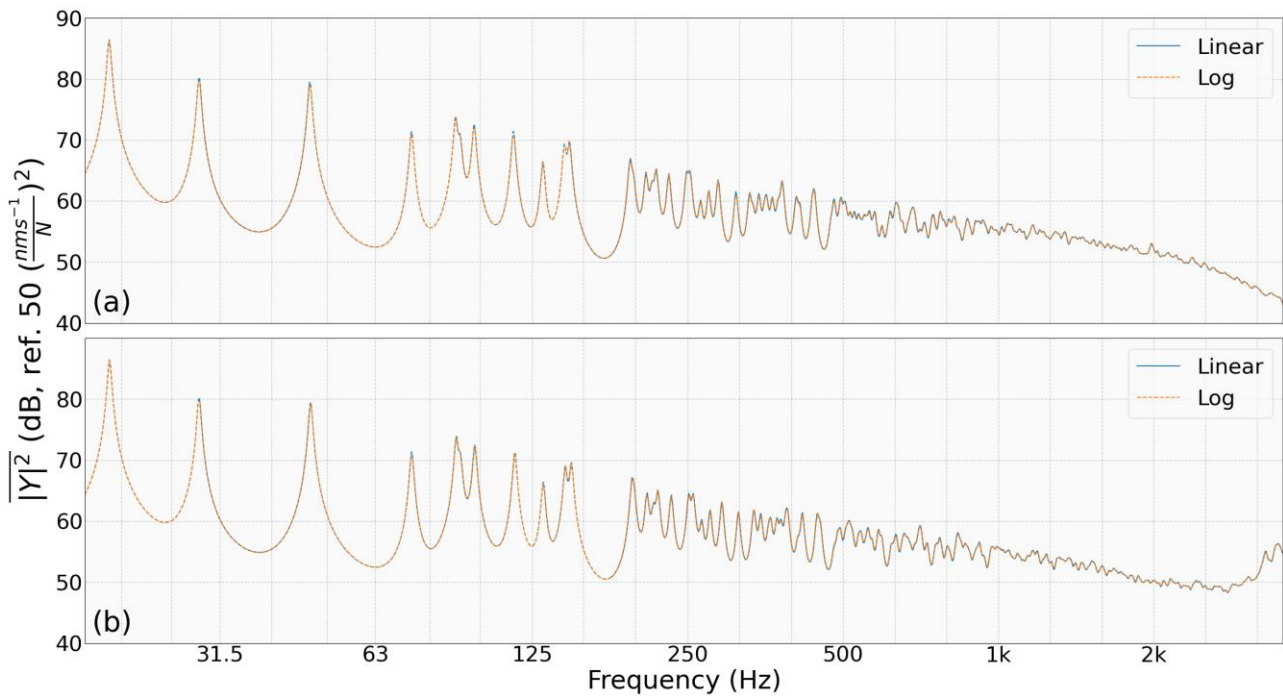


Figure 6 – Comparison of a high frequency resolution model with linear solution intervals and a model with logarithmic solution intervals. Spatially averaged squared transfer mobilities ($\overline{|Y|^2}$) from 17 Hz to 3654 Hz for F_1 . (a) SHELL281. (b) SOLID186.

Table 7 – Mode-Superposition method runtimes for SHELL281 and SHELL186 models on two different computers with logarithmic solution intervals.

Element Type	Runtime (hr:min)	
	Computer A	Computer B
SHELL281	0:12	0:06
SOLID186	1:07	0:34

5 Conclusion

This contribution has demonstrated experimentally validated and computationally efficient broadband models for CLT plates in the context of building acoustics. The study considered a frequency range until 3564 Hz, the upper bound of the nominal 3000 Hz one-third octave band.

On a several year-old CPU, the runtime optimised shell element model required 12 minutes and at least 638 MB RAM to solve. The runtime optimised solid element model required 67 minutes and at least 8.20 GB RAM to solve. On a one-and-a-half year-old CPU, the runtime improved by a factor of two, to 6 and 34 minutes

for the shell and solid models respectively. Overall, the optimised shell element model ran 498 times faster and required one-twentieth the RAM of the reference full solution method solid model.

In terms of accuracy, the shell element elements were accurate until approximately 2800 Hz, approximately the upper bound of the nominal 2500 Hz one-third octave band. Beyond 2800 Hz, the influence of the thickness modes were found to be non-negligible and must be taken into account with the use of solid elements. The solid elements were found to be stiffer than the shell elements for the low-frequency range, likely due to having just translational degrees of freedom while the shell elements have both translational and rotational degrees of freedom. The solid elements were also found to be slightly more accurate than the shell elements for the mid-frequency range, however less accurate for the upper mid- and lower high-frequency range.

Lastly, this study has implicitly demonstrated the flexibility and accuracy of layerwise models. The material properties of the CLT plate were input on a layerwise basis with shell elements governed by first-order shear deformations and layered quadratic solid elements. These models were each validated for the low-, mid-, and high-frequency ranges. Excluding the inability of the shell model to account for thickness modes, no large differences were observed between the shell and solid element models.

Such computationally efficient and flexible models can serve as a base for more complex assemblies involving CLT and/or increase the likelihood of dissemination of CLT prediction tools in industry. The shell element model in particular, will comfortably run on the average modern day laptop or PC. When the nominal 3000 Hz one-third octave band or above is critical, then a modern workstation and the use of solid elements is required. Further, the layerwise implementation of the models, allows flexibility in their potential extension to arbitrary stacking sequences, ply orientations, thicknesses and geometries with validated layerwise material properties.

Acknowledgements

The authors gratefully acknowledge the financial support of the research project by the Swiss Federal Office for Environment under their Environmental Technology Promotion program.

References

- [1] Espinoza, O.; Trujillo, V.R.; Mallo, M.F.L.; Buehlmann, U. Cross-laminated timber: Status and research needs in Europe. *BioResources* Vol 11(1), 2016, pp 281-295.
- [2] Hu, L.; Dagenais, C.; Qian, C.; Gagnon, S. Key parameters for impact and airborne noise control in wood buildings. In: *2020 International Congress on Noise Control*. Seoul, Korea, August 23-26, 2020, In CD-ROM.
- [3] Jayalath, A.; Navaratnam, S.; Gunawardena, T.; Mendis, P.; Aye, L.; Airborne and impact sound performance of modern lightweight timber buildings in the Australian construction industry. *Case Studies in Construction Materials*, Vol 15, 2021, pp e00632
- [4] Winter, C.; Buchschmid, M; Müller, G. Modeling of orthotropic plates out of cross laminated timber in the mid and high frequency range. *Procedia engineering*, Vol 199, 2017, pp 1392-1397.
- [5] Yang, Y.; Fenemore, C.; Kingan, M.J.; Mace, B.R. Analysis of the vibroacoustic characteristics of cross laminated timber panels using a wave and finite element method. *Journal of Sound and Vibration*, Vol 494, 2021.
- [6] Cremer, L.; Heckl, M.; Petersson, B.A.T. *Structure-borne sound: Structural vibrations and sound radiation at audio frequencies*. Springer, 3rd edition, 2013.
- [7] Ansys Mechanical APDL 2020R2 Documentation. *7 Element Library*. Element reference, ANSYS, Inc , 2021.